PROCEEDINGS OF SCIENCE

# Measurement of Quarkonium Production with CMS in pp Collisions at $\sqrt{s}$ = 7 TeV

**Andrew York*** **on behalf of The CMS Collaboration**
*CERN, PH Division, 1211 Geneve 23, Switzerland*
*University of Tennessee, Department of Physics, 1408 Circle Drive, Knoxville, TN, USA*
*E-mail:* Andrew.York@cern.ch

This talk presents quarkonium production rates in pp collisions at $\sqrt{s} = 7$ TeV as measured by the Compact Muon Solenoid (CMS) detector, with samples corresponding to an integrated luminosity of 36 pb$^{-1}$ and 4.6 fb$^{-1}$. We show official results for $J/\psi$, $\psi(2S)$, and $\Upsilon$ production as a function of transverse momentum, as well as results for relative prompt production of $\chi_{c2}$ and $\chi_{c1}$, and the first observation in CMS of the decays $B_c \to J/\psi\pi^{\pm}$ and $B_c \to J/\psi\pi^{\pm}\pi^{\mp}\pi^{\pm}$.

*XXI International Workshop on Deep-Inelastic Scattering and Related Subject -DIS2013,*
*22-26 April 2013*
*Marseilles,France*

*Speaker.

 

PoS(DIS 2013)295

## 1. Introduction

Understanding quarkonium production is a challenge for modern theories of fundamental particle interaction. Measured $J/\psi$ production rates at the Tevatron [1] were found to disagree with next-to-leading order nonrelativistic quantum chromodynamics (NLO NRQCD) color singlet predictions by about a factor of 50 [2]. It is therefore important to measure the production of quarkonium states as a test of modern theoretical models.

A detailed description of the CMS apparatus is given in Ref. [3]. The detectors most relevant for the results described here are the silicon tracker and muon detector systems. The central feature of the CMS apparatus is a superconducting solenoid of 6m internal diameter. Within the field volume are a silicon pixel and strip tracker, crystal electromagnetic calorimeter and brass/scintillator hadron calorimeter. In addition to the barrel and endcap detectors, CMS has extensive forward calorimetry. The inner tracker measures charged particles within the pseudorapidity range $|\eta| < 2.5$, where $\eta = -\ln(\tan(\theta/2))$, and $\theta$ is the polar angle measured from the beam axis. It provides an impact parameter resolution of 15 $\mu$m.

Muons are measured in gas ionization detectors embedded in a steel return yoke in the pseudorapidity range $|\eta| < 2.4$. The muon systems use three gas ionization technologies: drift tubes, cathode strip chambers, and resistive plate chambers. Matching the muons to tracks measured in the silicon tracker results in a transverse momentum, $p_T$, resolution between 1 and 1.5% for $p_T$ values up to 50 GeV/c. The first level (L1) of the CMS trigger system, composed of custom hardware processors, uses information from the calorimeters and muon detectors to select interesting physics events. The high-level trigger (HLT) processor farm further decreases the event rate from around 100 kHz to around 300 Hz, before data storage.

All of the analyses described in the subsequent sections extract signal yield using a maximum likelihood fit to dimuon or dimuon + $\gamma$ invariant mass distributions (in the case of prompt and non-prompt $\psi$, also the proper decay lengths). The efficiency is calculated from data control samples applying the Tag and Probe technique [4]; it is independent of production model and detector simulation. The detector acceptance is obtained from simulations assuming unpolarized production, with the possible effects of polarization accounted for as systematic uncertainty. The details of these techniques are given in the cited papers, but not discussed here.

## 2. J/$\psi$ and $\psi$(2S) Production

The total charmonium production cross section is determined from the yield in bins of the quarkonium transverse momentum, $p_T$, after correction for the average efficiency and acceptance in that bin, as well as normalization to luminosity and the decay branching fraction [5]. Signal and background yields are obtained from unbinned maximum likelihood fits to dimuon invariant mass and the proper decay length. Figure 1 shows the measured cross sections for prompt $J/\psi$ and $\psi(2S)$ as a function of $p_T$. It also compares the measured results with theoretical predictions from NRQCD. The NRQCD prediction includes non-prompt production in the $J/\psi$ case caused by feed-down decays from heavier charmonia, and can therefore be directly compared with the data. The prompt $J/\psi$ and $\psi(2S)$ cases show good agreement with theoretical predictions. The $\psi(2S)$ case has particularly good agreement, as theoretical uncertainties are lower due to the absence of

feed-down from heavier charmonium states. The NRQCD theoretical uncertainties shown in the figure include those feed-down contributions from the colour-octet, long-distance matrix elements determined by fits to Tevatron data [6]. The cross section results assume isotropic decays in the production, as well as four other polarization scenarios. Figure 2 shows the measured cross section for non-prompt $J/\psi$ and $\psi(2S)$ production compared to theoretical predictions from FONLL [8, 9]. The measurements lie systematically below FONLL predictions, possibly because of the large uncertainty on the $BF(B \to \psi(2S)X)$ branching fraction. In general, for both non-prompt states, the observed differential cross sections seem to fall more rapidly than the FONLL prediction at high $p_T$. In addition, the inclusive branching fraction $BF(B \to \psi(2S)X)$ is extracted from the ratio of the non-prompt cross sections to be:

$$BF(B \to \psi(2S)X) = (3.08 \pm 0.12\ (stat.+syst.) \pm 0.13\ (theor.) \pm 0.42\ (BF_{PDG})) \cdot 10^{-3} \quad (2.1)$$

improving the relative uncertainty of the previous world average by a factor of three.

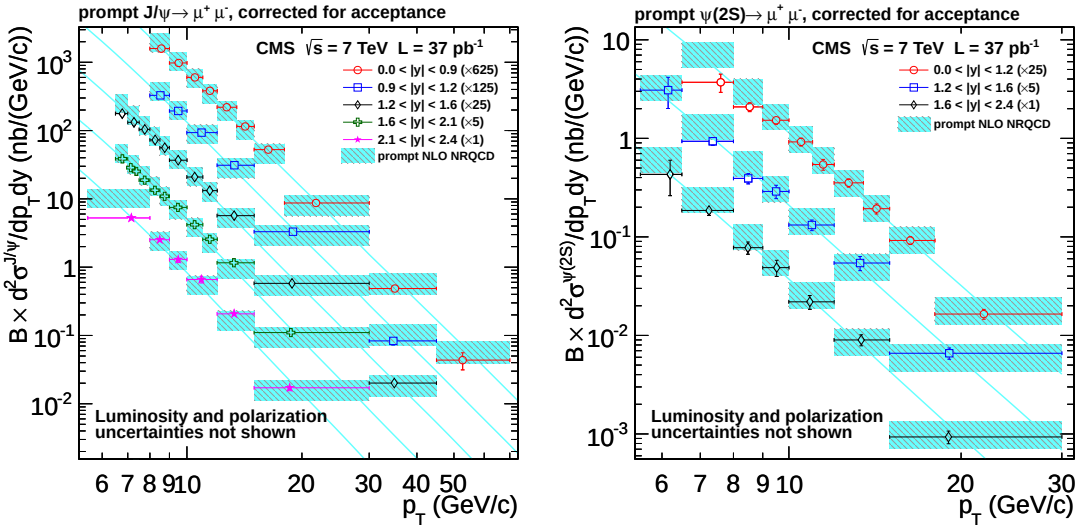


Figure 1: Measured differential cross section for *prompt* $J/\psi$ (left) and $\psi(2S)$ production (right) as a function of $p_T$ for different rapidity bins [5]. The error bars on the data points include statistical and systematic contributions except luminosity and polarization. The measurements have been offset by the numerical values given in the legend for easier viewing. The coloured (dark) bands indicate the theoretical predictions from NRQCD calculations [6]. The lines are only added for illustrative purposes.

## 3. $\Upsilon$(nS) Production

The $\Upsilon(1S)$, $\Upsilon(2S)$, and $\Upsilon(3S)$ production cross sections are determined using an integrated luminosity of $36 \pm 1.4\ \text{pb}^{-1}$ [7]. $\Upsilon$ resonances are identified via their decays into oppositely charged muons. Integrated over the range $p_T^{\Upsilon} < 50$ GeV/c and rapidity $|y^{\Upsilon}| < 2.4$ and assuming unpolarized $\Upsilon$ production, the $\Upsilon$ production cross sections times dimuon branching fractions are:

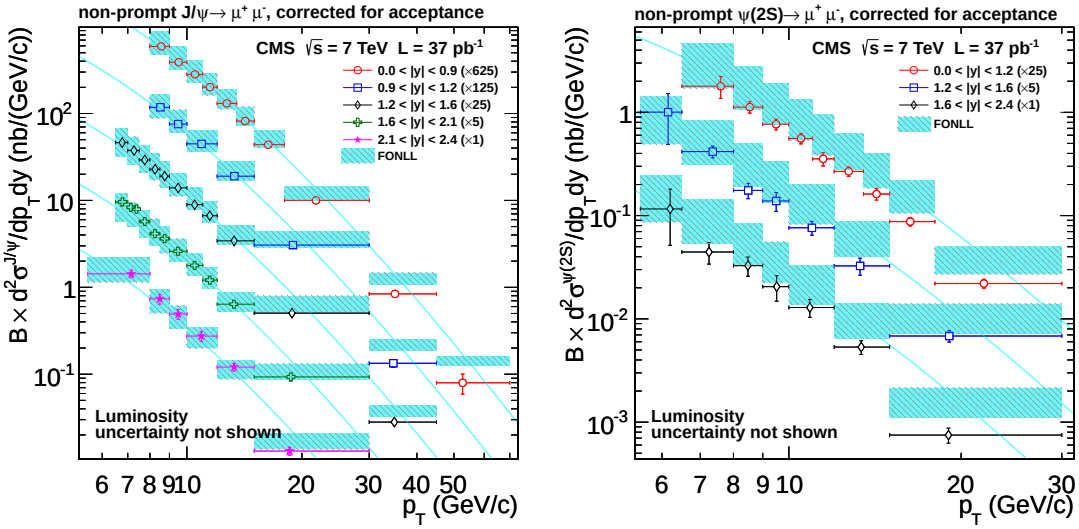


Figure 2: Measured differential cross section for *non-prompt* $J/\psi$ (left) and $\psi(2S)$ (right) production as a function of $p_T$ for different rapidity bins [5]. The error bars on the data points include statistical and systematic contributions except luminosity. The measurements have been offset by the numerical values given in the legend for easier viewing. The coloured (dark) bands indicate the theoretical predictions from FONLL calculations [8, 9]. The lines are only added for illustrative purposes.

- $\sigma(pp \to \Upsilon(1S)X \cdot BF(\Upsilon(1S) \to \mu^+\mu^-)) = (8.55 \pm 0.05^{+0.56}_{-0.50} \pm 0.34)\text{nb}^{-1}$,
- $\sigma(pp \to \Upsilon(2S)X \cdot BF(\Upsilon(2S) \to \mu^+\mu^-)) = (2.21 \pm 0.03^{+0.16}_{-0.14} \pm 0.09)\text{nb}^{-1}$,
- $\sigma(pp \to \Upsilon(3S)X \cdot BF(\Upsilon(3S) \to \mu^+\mu^-)) = (1.11 \pm 0.02^{+0.10}_{-0.08} \pm 0.04)\text{nb}^{-1}$,

where the first uncertainty is statistical, the second is systematic, and the third is from the uncertainty in the integrated luminosity. The dominant sources of systematic uncertainty in the cross section measurements arise from the data-driven determination of the muon identification and trigger efficiencies, the correction factor for the efficiencies, and the integrated luminosity. Figure 3 shows the measured differential cross sections in bins of transverse momentum and rapidity.

Figure 4 compares differential $\Upsilon(nS)$ cross section results as a function of rapidity to measurements made by the LHCb Collaboration [10] (left plot) and as a function of $p_T^{\Upsilon(1S)}$ to various theoretical models (right plot). The rapidity coverage of LHCb is mostly complementary to that of CMS. In the single bin of overlapping coverage, the measurements of each experiment agree within the experimental error. The comparison to theory includes the following models: the CASCADE MC generator [11], normalized PYTHIA [12], NRQCD at next-to-leading order (NLO) including feed-down and incorporating color-singlet and color-octet contributions [13], the color-singlet model (CSM) to NLO and NNLO* with feed-down accounted for by scaling the $\Upsilon(1S)$ direct-production cross section by a factor of 2 [14]. The theoretical predictions are based on published models for unpolarized $\Upsilon(1S)$ production and, except for NRQCD, were made for lower energy but updated by the authors [7] to $\sqrt{s} = 7$ TeV.

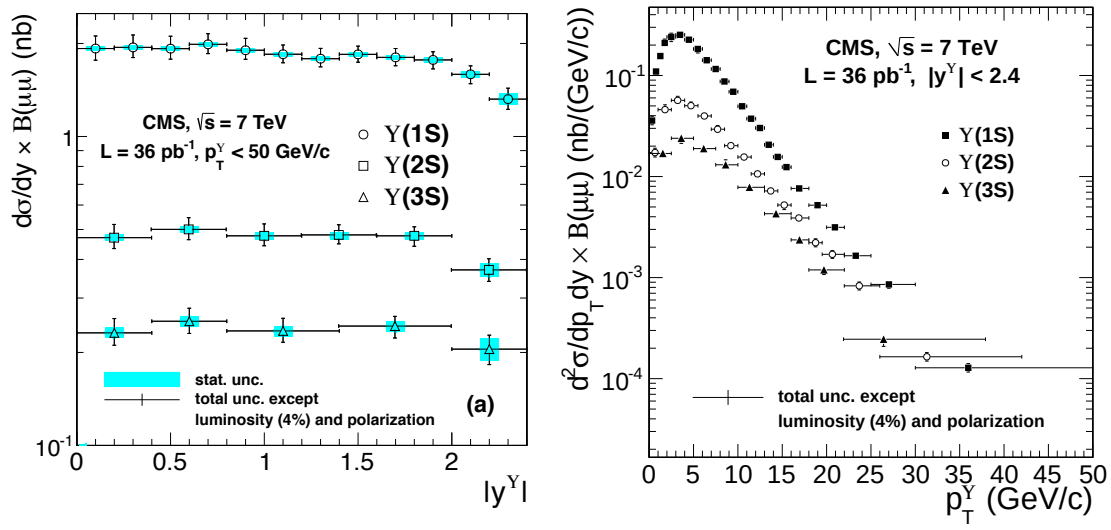


Figure 3: Acceptance-corrected differential $\Upsilon(nS)$ cross sections as a function of rapidity in the $p_T^\Upsilon < 50$ GeV/c range (left) and as a function of $p_T^\Upsilon$ in the rapidity range $|y^\Upsilon| < 2.4$ (right) [7]. Error bars represent the total uncertainty except uncertainty due to the $\Upsilon(nS)$ polarization and integrated luminosity, and the bands in the left plot represent only statistical uncertainty.

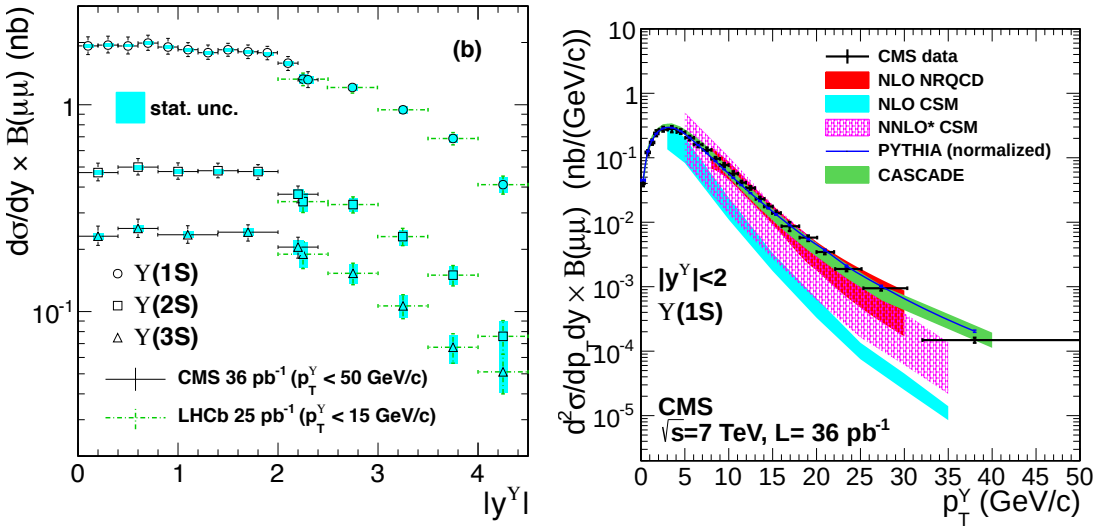


Figure 4: Acceptance-corrected differential $\Upsilon(nS)$ cross section as a function of rapidity in the $p_T^\Upsilon < 50$ GeV/c range compared to LHCb results [10] (left) and differential $\Upsilon(1S)$ cross section as a function of $p_T^\Upsilon$ in the rapidity range $|y^\Upsilon| < 2$ compared to various theoretical models (right) [7]. For measured results, bands represent statistical uncertainty and bars represent total experimental uncertainty (except for uncertainty due to $\Upsilon(nS)$ polarization). For theoretical models, bands represent the uncertainty of the prediction quoted by the author of the model.

## 4. Relative Prompt Production Ratio $\chi_{c2}/\chi_{c1}$

The ratio of the prompt $\chi_{c2}$ to $\chi_{c1}$ cross section is measured to include both directly produced $\chi_c$ mesons and indirectly produced ones from the decays of intermediate states [15]. $\chi_{c1}$ and $\chi_{c2}$ candidates are selected by searching for their radiative decays into the $J/\psi+\gamma$ final state, with the $J/\psi$ decaying into two muons. All candidates must fall within the acceptance region $p_T(\gamma) > 0.5$ GeV/c and $|y(J/\psi)| < 1.0$. An unbinned maximum likelihood fit to the $\mu^+\mu^-\gamma$ invariant mass extracts the $\chi_{c1,2}$ yield in bins of $p_T(\chi_{c1,2})$. This signal yield is corrected for the average acceptance and efficiency in each bin.

The comparison of the measured production ratio (which includes feed-down) with theoretical models that do not include feed-down requires knowledge of the amount of feed-down from all possible short-lived intermediate states that can decay into $\chi_{c2}$ or $\chi_{c1}$. The largest known such contribution originates from $\psi(2S)$ decays, and can be estimated using the measured prompt $J/\psi$ and $\psi(2S)$ cross sections in pp collisions at 7 TeV [5], the world average branching fractions for the decays $\psi(2S) \to \chi_{c1,2}+\gamma$, and assuming the same fractional $\chi_c$ contribution to the total prompt $J/\psi$ production cross section as measured in pp collisions at 1.96 TeV [16]. This method of estimation finds that roughly 5% of both the prompt $\chi_{c1}$ and $\chi_{c2}$ samples originate from $\psi(2S)$ decays.

Figure 5 compares the measured production times branching fraction ratio with theoretical predictions derived from the $k_T$-factorization [17] and NRQCD [18] calculations. The theoretical calculation for the $k_T$-factorization approach is given in the same kinematic range ($p_T(\gamma) > 0.5$ GeV/c, $|y(J/\psi)| < 1.0$) as the CMS measurement. The prediction from NRQCD is given in the kinematic range $p_T(\gamma) > 0$ GeV/c, $|y(J/\psi)| < 1.0$. A small correction factor (ranging from 0.98 to 1.02 depending on $p_T$, with uncertainties from 1 to 4%) is derived from MC simulation to extrapolate the phase space of the CMS measurement to the one used for the theoretical calculation. The $k_T$-factorization prediction agrees well with the shape of the measured ratio, but with a global normalization that is higher by about a factor of two with respect to the measurement. It is worth noting that this calculation assumes the same wave function for the $\chi_{c1}$ and the $\chi_{c2}$. On the other hand, the NRQCD prediction agrees with data within the experimental and theoretical uncertainties. Predictions for $\chi_{c1}$ or $\chi_{c2}$ polarizations in NRQCD were not provided though, so the level of agreement can vary according to the polarization assumption.

## 5. Observation of the decay $B_c \to J/\psi\pi^\pm$ and $B_c \to J/\psi\pi^\pm\pi^\mp\pi^\pm$

Figure 6 shows the first CMS observation of the decays $B_c \to J/\psi\pi^\pm$ and $B_c \to J/\psi\pi^\pm\pi^\mp\pi^\pm$ in 4.7 fb$^{-1}$ of 2011 LHC data collected with displaced dimuon vertex triggers [19]. A maximum likelihood fit extracts a $B_c \to J/\psi\pi^\pm$ yield of $330 \pm 41\ (stat.) \pm 23\ (syst.)$ events and a $B_c \to J/\psi\pi^\pm\pi^\mp\pi^\pm$ yield of $108 \pm 19\ (stat.) \pm 14\ (syst.)$ events.

## 6. Summary

Several quarkonium resonances with decays into muons have been studied with the CMS detector at the LHC. The excellent performance of the detector results in competitive measurements providing valuable input for production model builders.

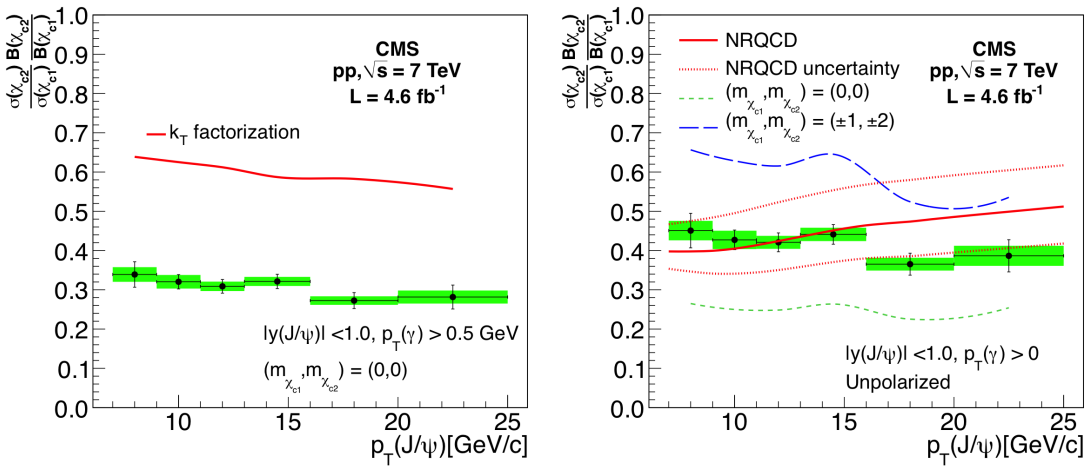


Figure 5: Comparison of the measured $\frac{\sigma(\chi_{c2})BF(\chi_{c2})}{\sigma(\chi_{c1})BF(\chi_{c1})}$ [15] with theoretical predictions from the $k_T$-factorization[17] (left) and NRQCD[18] (right). Solid red lines represent the prediction, green bands represent statistical uncertainty, and error bars represent statistical and systematic uncertainty. Predictions from both theoretical models assume unpolarized $\chi_c$ for the basic comparison, but the NRQCD comparison also shows the results of two different extreme polarization scenarios as long-dashed blue and short-dashed green lines. The 1-standard-deviation uncertainties in the NRQCD prediction (dotted red lines) originate from uncertainties in the color-octet matrix elements.

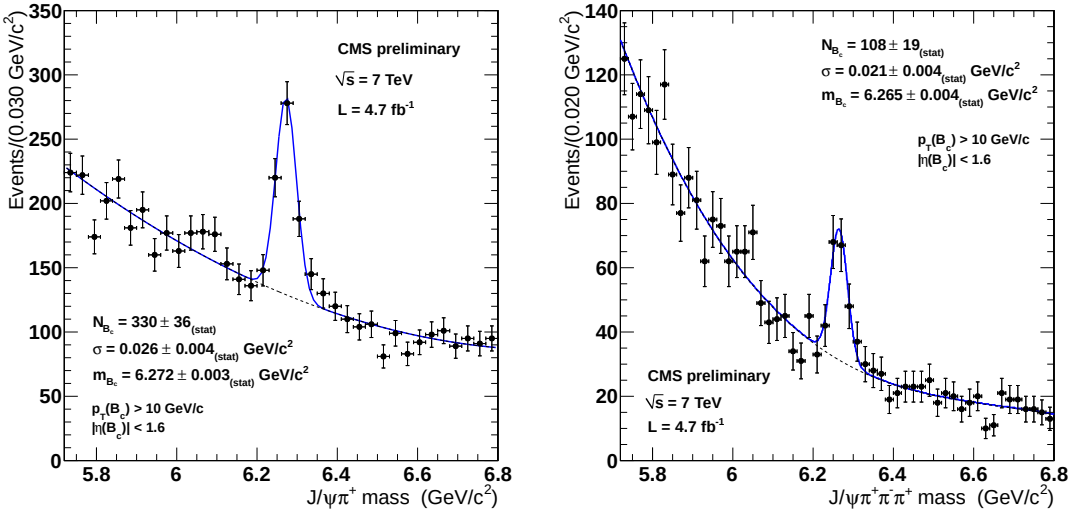


Figure 6: Invariant mass yields for $B_c \to J/\psi\pi^{\pm}$ (left) and $B_c \to J/\psi\pi^{\pm}\pi^{\mp}\pi^{\pm}$ (right) candidates [19].

## References


[1] F. Abe et al., CDF Collaboration, Phys. Rev. Lett. **69**, 3704 (1992)

[2] M. Kramer, 1, Prog. Part. Nucl. Phys. **47**, 141 (2001) [hep-ph/0106120].

[3] S. Chatrchyan *et al.* [CMS Collaboration], JINST **3**, S08004 (2008).

[4] [CMS Collaboration], CMS-PAS-TRK-10-002.

[5] S. Chatrchyan *et al.* [CMS Collaboration], JHEP **1202**, 011 (2012) [arXiv:1111.1557 [hep-ex]].

[6] Y. -Q. Ma, K. Wang and K. -T. Chao, Phys. Rev. Lett. **106** (2011) 042002 [arXiv:1009.3655 [hep-ph]].

[7] S. Chatrchyan *et al.* [CMS Collaboration], arXiv:1303.5900 [hep-ex].

[8] M. Cacciari, M. Greco and P. Nason, JHEP **9805**, 007 (1998) [hep-ph/9803400].

[9] M. Cacciari, S. Frixione and P. Nason, JHEP **0103**, 006 (2001) [hep-ph/0102134].

[10] RAaij *et al.* [LHCb Collaboration], Eur. Phys. J. C **72**, 2025 (2012) [arXiv:1202.6579 [hep-ex]].

[11] H. Jung, S. Baranov, M. Deak, A. Grebenyuk, F. Hautmann, M. Hentschinski, A. Knutsson and M. Kramer *et al.*, Eur. Phys. J. C **70**, 1237 (2010) [arXiv:1008.0152 [hep-ph]].

[12] M. Bargiotti and V. Vagnoni, CERN-LHCB-2007-042.

[13] K. Wang, Y. -Q. Ma and K. -T. Chao, Phys. Rev. D **85**, 114003 (2012) [arXiv:1202.6012 [hep-ph]].

[14] J. P. Lansberg, J. Phys. G **38**, 124110 (2011) [arXiv:1107.0292 [hep-ph]].

[15] S. Chatrchyan *et al.* [CMS Collaboration], Eur. Phys. J. C **72**, 2251 (2012) [arXiv:1210.0875 [hep-ex]].

[16] CDF Collaboration, Phys. Rev. Lett. **79**, 578 (1997)

[17] Baranov, S. P., Phys. Rev. D **83**, 034035 (2011)

[18] Y. -Q. Ma, K. Wang and K. -T. Chao, Phys. Rev. D **83**, 111503 (2011) [arXiv:1002.3987 [hep-ph]].

[19] CMS Collaboration, CMS-PAS-BPH-11-003, 2012